NEOPLASIA
www.neoplasia.com

Volume 20 Number 4 April 2018 pp. 387–400 387

Nephronectin is Correlated with Poor Prognosis in Breast Cancer and Promotes Metastasis via its Integrin-Binding Motifs

Tonje S. Steigedal[*,†,‡,§], Jimita Toraskar[*,§], Richard P. Redvers[†,¶], Marit Valla[*,#], Synnøve N. Magnussen[**], Anna M. Bofin[*], Signe Opdahl[#], Steinar Lundgren[*,††], Bedrich L. Eckhardt[‡‡,§§,¶¶], John M. Lamar[‡,##], Judy Doherty[†], Richard O. Hynes[‡,*], Robin L. Anderson[†,¶,†††,1] and Gunbjørg Svineng[**,1]**

*Department of Clinical and Molecular Medicine, Faculty of Medicine and Health Sciences, Norwegian University of Science and Technology (NTNU), Trondheim, Norway; [†]Peter MacCallum Cancer Centre, East Melbourne, Victoria, Australia; [‡]David H Koch Institute for Integrative Cancer Research, Massachusetts Institute of Technology, Cambridge, MA, United States; [§]Central Norway Regional Health Authority, Stjørdal, Norway; [¶]Olivia Newton-John Cancer Research Institute, Heidelberg, Victoria, Australia; [#]Department of Public Health and Nursing, Faculty of Medicine and Health Sciences, NTNU, Trondheim, Norway; **Department of Medical Biology, Faculty of Health Sciences, UiT - The Arctic University of Norway, Tromsø, Norway; [††]Cancer Clinic, St. Olav's Hospital, Trondheim University Hospital, Trondheim, Norway; [‡‡]Morgan Welch Inflammatory Breast Cancer Research Program and Clinic, The University of Texas at MD Anderson Cancer Centre, Houston, TX, USA; [§§]Section of Translational Breast Cancer Research, The University of Texas at MD Anderson Cancer Centre, Houston, TX, USA; [¶¶]Department of Breast Medical Oncology, The University of Texas at MD Anderson Cancer Centre, Houston, TX 77030, USA; [##]Department of Molecular and Cellular Physiology, Albany Medical College, Albany, NY, USA; [***]Howard Hughes Medical Institute, Massachusetts Institute of Technology, Cambridge, MA, United States; [†††]School of Cancer Medicine, La Trobe University, Bundoora, Victoria, Australia

Abstract

Most cancer patients with solid tumors who succumb to their illness die of metastatic disease. While early detection and improved treatment have led to reduced mortality, even for those with metastatic cancer, some patients still respond poorly to treatment. Understanding the mechanisms of metastasis is important to improve prognostication, to stratify patients for treatment, and to identify new targets for therapy. We have shown previously that expression of nephronectin (NPNT) is correlated with metastatic propensity in breast cancer cell lines. In the present study, we provide a comprehensive analysis of the expression pattern and distribution of NPNT in breast cancer tissue from 842 patients by immunohistochemical staining of tissue microarrays from a historic cohort. Several patterns of NPNT staining were observed. An association between granular cytoplasmic

Address all correspondence to: Tonje S. Steigedal, Department of Clinical and Molecular Medicine, Faculty of Medicine and Health Sciences, NTNU, Postbox 8905, N-7491 Trondheim, Norway. E-mail: Tonje.S.Steigedal@ntnu.no
[1] These authors contributed equally to the work.
Received 28 November 2017; Revised 17 February 2018; Accepted 19 February 2018

1476-5586
https://doi.org/10.1016/j.neo.2018.02.008

staining (in <10% of tumor cells) and poor prognosis was found. We suggest that granular cytoplasmic staining may represent NPNT-positive exosomes. We found that NPNT promotes adhesion and anchorage-independent growth via its integrin-binding and enhancer motifs and that enforced expression in breast tumor cells promotes their colonization of the lungs. We propose that NPNT may be a novel prognostic marker in a subgroup of breast cancer patients.

Neoplasia (2018) 20, 387–400

Introduction

Metastasis is the major cause of death for patients with solid tumors who succumb to their disease [1]. Breast cancer metastases usually develop in multiple organs including lymph nodes, bone, lung, liver, and brain [2]. Understanding the molecular mechanisms by which breast tumors metastasize is integral to improving outcome for patients with advanced disease. However, the metastatic process and the selective preference of tumor cells for certain tissues is complex and dependent on various factors including vascular patterns, adhesion factors, and tumor cell interactions with the stroma at the metastatic site [3].

Human breast cancer is heterogeneous and is divided into subgroups that vary in gene expression profiles, phenotype, aggressiveness, metastatic propensity, and response to treatment [4–6]. A comprehensive effort with screening programs, development of new chemotherapeutic and endocrine regimens, and implementation of targeted agents has contributed to reduced breast cancer mortality [4]. Stratification of patients into optimal treatment regimens is therefore of increasing importance. The four original molecular subtypes of breast cancer (Luminal, HER2-enriched, basal-like, and normal-like) [5,6] have subsequently been divided into additional subtypes that are likely to be of clinical relevance [4,7].

Nephronectin (NPNT), also known as POEM (Preosteoblast Epidermal Growth Factor (EGF)-like repeat protein with MAM domain,) was initially identified as a gene involved in embryonic development of endocrine organs via interactions with the integrin α8β1 receptor [8–10]. Structurally, NPNT has five EGF-like domains, a MAM (meprin, A5 protein and receptor protein tyrosine phosphatase) domain, and an RGD (Arg-Gly-Asp) integrin-binding motif and is generally proposed to be a secreted glycoprotein [8,10]. It is secreted by bulge stem cells in hair follicles and induces differentiation of arrector pili muscle cells [11,12]. NPNT also functions in differentiation of atrioventricular cells and in promotion of vascularization [13,14].

Few reports exist about the role of NPNT in tumor progression and metastasis. In a previous study of genes involved in metastatic processes, we analyzed primary tumors of mouse mammary tumor lines exhibiting various degrees of metastatic capacity and found a correlation between increased *Npnt* expression levels and metastatic propensity [15]. We went on to show that knockdown of NPNT in the highly metastatic 4T1.2 mammary tumor caused a significant reduction of metastasis to lung, spine, and kidney [15]. In addition, Borowsky et al. reported higher levels of NPNT in metastatic mammary tumor cells compared to nonmetastatic cells in a different syngeneic mouse model of breast cancer, supporting a putative role of NPNT as a metastasis-promoting factor [16].

This study reports the first large-scale analysis of NPNT protein expression in human breast cancer. By immunohistochemistry (IHC), we found several different staining patterns for NPNT. Granular cytoplasmic staining was associated with poor prognosis and may be consistent with tumor cell–derived extracellular vesicles. Using preclinical models, we show the necessity of the NPNT integrin-binding site in the metastatic process. Our functional data demonstrate that the disruption of the integrin-binding site within NPNT can modulate the propensity of metastatic breast cancer cells to adhere to and colonize the lung. Collectively, our data identify a functional role for NPNT during metastasis and describe its expression and possible prognostic role in a large cohort of breast cancer patients.

Materials and Methods

Patients

The study population has been described previously in detail [17]. Briefly, of a total of 1393 new cases of breast cancer occurring between 1961 and 2008, 909 cases were available for subtyping using IHC and *in situ* hybridization (ISH) markers as surrogates for gene expression analyses, and 886 of these were assembled in tissue microarrays (TMAs). Patients were followed until death from breast cancer or from other causes, as registered by the Cause of Death Registry, or until December 31, 2010. Only cases in TMAs were included in the present study, and 842 cases were suitable for analysis. Two subtypes, 5 negative phenotype and basal-like phenotype described in Engstrom et al., were merged into triple negative in the current analysis [17]. The study was performed in accordance with the approval granted by the Regional Committee for Medical and Health Research Ethics (REK Midt-Norge, ref. no.:836/2009), and dispensation from the requirement of patient consent was granted.

Immunostaining (IHC and IF)

The patient samples were fixed in formalin, but details of the preanalytical conditions are unknown as these samples were collected over several decades. From TMAs, 4-μm–thick sections were cut and mounted on Superfrost+ glass slides, dried overnight at 37°C, and stored in the freezer at −20°C. Before IHC, slides were heated for 2 hours at 60°C and pretreated in a PT Link Pre-Treatment Module for Tissue Specimens (Dako Denmark A/S, 2600 Glostrup, DK) with buffer (High pH Target Retrieval Solution K8004) for 20 minutes at 97°C. Immunostaining for NPNT (Atlas Antibodies/Sigma Cat.: HPA003711, Lot No.: D97165, dilution 1:100) was done in a DakoCytomationAutostainer Plus (Dako) at 4°C overnight. Dako REAL EnVision Detection System with Peroxidase/DAB+, Rabbit/Mouse, code K5007, was used for visualization. The following controls were used: a negative control (omitting the primary antibody), rabbit IgG isotype control, and a positive control (normal kidney). Sections from validation and optimization of the anti-NPNT

antibody (Atlas Antibodies/Sigma) on human tissues are shown in Supplementary Figure S1. The figure shows that the optimal dilution of the antibody was 1:100 in the human samples.

All mouse tissues subjected to immunostaining analyses were fixed in 10% buffered formalin for about 24 hours and embedded in paraffin following standard procedures. Tissue blocks were sectioned at 4 μm and rehydrated through Neo-clear and ethanol series. Antigen retrieval was performed in 10 mM EDTA (pH 9) by 15-minute boiling in a microwave oven. Primary antibodies; anti-human NPNT (Atlas Antibodies/Sigma, Cat.: HPA003711, Lot No.: D97165, dilution 1:150), anti-mouse NPNT (Abnova, Cat.: PAB8467, Lot No.: TG 100309, dilution 1:150), anti-V5 (CST, Cat.: 13202S, Lot No.: 2, dilution 1:150), anti-collagen V (Abcam, Cat.: ab7046, Lot No.: GR222605-7, dilution 1:200), anti-Fibronectin (Abcam, Cat.: ab2413, Lot No.: GR250744-3, dilution 1:200), and Rabbit IgG Isotype control (BD Biosciences, Cat.: 610822, Lot No.: 7069938). All antibodies were incubated at 4°C overnight. Secondary antibodies were used according to manufacturer's recommendations (Dako EnVision, Glostrup, Denmark). IF detection was performed using anti-CHMP4B (Atlas Antibodies/Sigma, Cat.: HPA051751, Lot No.: R67106, dilution 1:300, anti-V5 (CST, Cat.: 13202S, Lot No.: 2, dilution 1:150) and secondary antibodies; Goat anti-Mouse IgG (H+L) Highly Cross-Adsorbed Secondary Antibody, Alexa Fluor Plus 647, (Thermo Fisher Scientific, Cat.: A32728, Lot No.: RJ243424, dilution 1:1000) and Goat anti-Rabbit IgG (H+L) Highly Cross-Adsorbed Secondary Antibody, Alexa Fluor Plus 488 (Thermo Fisher Scientific, Cat.: A32731, Lot No.: RJ243417, dilution 1:1000). Validation of specificity of the anti-human NPNT (Atlas Antibodies/Sigma and anti-mouse NPNT (Abnova) antibodies on MMTV-PyMT mouse tissues is shown in Supplementary Figure S2.

Scoring, Reporting, and Classification of the Human Patient Samples

All TMA slides were digitized for review as described previously after both hematoxylin-eosin-saffron (HES) and IHC staining [17]. Each case was assessed by two researchers independently (by T.S.S. and A.M.B. or M.V.), one of whom (A.M.B. and M.V.) was a pathologist. Discrepant results were discussed, and consensus was reached. For diffuse cytoplasmic staining, a staining index was calculated by multiplying staining intensity by the proportion of stained cells. Staining intensity was recorded as follows: 0 (no staining), 1 (weak), 2 (moderate), and 3 (strong). The proportion of stained cells was scored as 0 (<1%), 1 (1-<10%), 2 (≥10-<50%), and 3 (≥50%). A staining index of 0-2 was interpreted as negative; 3-9, as positive. For granular cytoplasmic staining, any staining was interpreted as positive, and the proportion of stained cells was recorded as <1%, 1-<10%, ≥10-<50%, and ≥50%. The presence of scattered, strongly cytoplasmic stained tumor cells was recorded. Nuclear staining in ≥1% of tumor cells was interpreted as positive.

MMTV-PyMT Transgenic Animals

Breast tumor tissues and lungs from MMTV-PyMT animals (The Jackson Laboratory, ME, USA) were collected to represent different tumor stages and used for IHC and ISH analysis, in addition to isolation of primary cells. IHC-stained samples were assessed (by T.S.S. and J.T.) using the same scoring system as for the human samples. Mice were housed Comparative Medicine Core Facility at NTNU, and the studies were approved by The Norwegian Food Safety Authority (FOTS number 3683) and conducted in accordance with the institutional animal ethics guidelines.

Cell Culture

The mouse cell lines 67NR, 168FARN, 66cl4, 4TO7, and 4T1 were kindly provided by Dr. Fred Miller (Wayne State University, Detroit, MI) and have been described previously [18]. These cells, and the 4T1-shNPNT cells, were cultured in DMEM (Gibco, Invitrogen, Carlsbad, CA) supplemented with 10% fetal calf serum (FCS, Bovogen, VIC, Australia) and 1% (v/v) penicillin-streptomycin. 66cl4-cells with stable expression of mCherry were made as described previously [19] and cultured in α-MEM containing 5-10% FCS and 1% (v/v) penicillin-streptomycin. Cell lines are routinely tested for mycoplasma infection. In addition, a comprehensive screening for viral and bacterial pathogenic contamination was performed at Laboratorio Dynamimed, Madrid, prior to the animal experiments. Additional information about the 66cl4-NPNT and 4T1-shNPNT is described in supplementary material.

Tumor Growth and In Vivo Lung Colonization Assay

Female BALB/c mice (6-8 weeks old, Walter and Eliza Hall Institute, Melbourne, Australia, or from Taconic M&B, Skensved, Denmark) were anesthetized and injected either orthotopically into the mammary gland (1×10^5 cells) or intravenously into the tail vein (5×10^5 cells) with various mCherry-expressing 66cl4-cell line variants as described previously [15]. Mice bearing mammary tumors were culled after 35 days. Relative tumor burden (RTB) was measured based on the level of genomic DNA for mCherry compared to that of vimentin [20]. Primary tumors were collected and subjected to IHC analyses. Following intravenous injection, mice were monitored daily and sacrificed after 3 weeks. Lungs were collected and subjected to RTB, IHC, and IF analyses. Representative left lung lobes from the lung colonization assay were imaged using the EVOS FL Auto Cell Imaging System. Each image was created using a stitch of several images to cover the entire lung lobe. Mice were housed either in the Peter MacCallum Animal Care Facility or in the Comparative Medicine Core Facility at NTNU, and all animal studies were approved by either the Peter MacCallum Animal Ethics Committee (AEEC project number E411) or The Norwegian Food Safety Authority (FOTS number 4551) and conducted in accordance with the institutional animal ethics guidelines.

Isolation of Epithelial Cells

Primary epithelial cells were isolated from FVB wild-type and MMTV-PyMT transgenic mice [21]. Normal and tumor mammary tissues were minced in 5 ml DMEM/F12 (Gibco) with 2% FCS (Invitrogen), 10 mM HEPES, 10 ng/ml epidermal growth factor, 10 μg/ml insulin, 10 mg/ml BSA, 2 mM glutamine, 50 U/ml penicillin, 50 μg/ml streptomycin sulfate, and 1.5 mg/ml collagenase type IA-S (Sigma) for 3 hours at 37°C with gentle rotation. Cells were spun at 1600 rpm for 4 minutes and resuspended in trypsin prior to a second spin at 1400 rpm and resuspension in fresh medium without collagenase. Cells were incubated at 37°C with 5% CO_2 for about 2-3 weeks.

Quantitative Real-Time PCR (qRT-PCR)

Total RNA was isolated using the RNeasy kit (Qiagen, Germantown, MD) and cDNA synthesized using the First-Strand cDNA Synthesis Kit (Promega, Madison, WI). qRT-PCRs were performed using Bio-Rad SYBR Green Supermix (Bio-Rad, Hercules, CA) according to the manufacturer's instructions and analyzed using Bio-Rad Software. NPNT expression was normalized to Cdc40 and Csnk2a2 (geNormPLUS, Southampton, United Kingdom).

Table 1. Patient and Tumor Characteristics, and Risk of Death from Breast Cancer According to NPNT Positive Staining Pattern

Patient and Tumor Characteristics	NPNT Phenotype Positive Cases						All Cases[d]
	Nuclear Staining[a]	Diffuse Cytoplasmic Staining[b]	Single Cells Positive	Granular Cytoplasmic Staining[c]	Granular Cytoplasmic Staining <10%	Granular Cytoplasmic Staining ≥10%	
Number of cases (%)	385 (45.7)	424 (50.4)	129 (15.3)	116 (13.8)	60 (7.1)	56 (6.7)	842
Mean age at diagnosis (SD)	73.0 (9.7)	72.6 (9.8)	71.3 (10.4)	72.8 (9.3)	72.3 (9.2)	73.3 (9.4)	72.0 (10.4)
Stage at diagnosis (%, 95% CI)							
I	180 (44, 39-49)	200 (49, 44-54)	74 (18, 14-22)	62 (15, 12-19)	29 (7, 5-10)	33 (8, 5-11)	411 (49)
II	158 (47,42-53)	178 (53, 48-59)	42 (13, 9-16)	41 (12, 9-16)	23 (7, 4-10)	18 (5, 3-8)	333 (40)
III	26 (51, 37-65)	21 (41, 28-55)	6 (12, 3-21)	7 (14, 4-23)	5 (10, 2-18)	2 (4, 0-9)	51 (6)
IV	20 (49, 33-64)	24 (59, 43-74)	7 (17, 5-29)	6 (15, 4-26)	3 (7, 0-15)	3 (7, 0-15)	41 (5)
Lymph node status at diagnosis (%, 95% CI)							
Positive	141 (47, 42-53)	152 (51, 45-57)	39 (13, 9-17)	35 (12, 8-15)	22 (7, 4-10)	13 (4, 2-7)	297 (35)
Negative	129 (49, 43-55)	139 (53, 47-59)	48 (18, 14-23)	37 (14, 10-18)	13 (5, 2-8)	24 (9, 6-13)	264 (31)
Negative, <5 nodes[e]	30 (45, 33-58)	31 (47, 35-59)	13 (20, 10-29)	11 (17, 8-26)	7 (11, 3-18)	4 (6, 0-12)	66 (8)
Unknown	85 (40, 33-46)	102 (47, 41-54)	29 (13, 9-18)	33 (15, 11-20)	18 (8, 5-12)	15 (7, 4-10)	215 (26)
Molecular subtype (%, 95% CI)							
Luminal A	202 (50, 45-55)	191 (47, 42-52)	43 (11, 8-14)	45 (11, 8-14)	22 (5, 3-8)	23 (6, 3-8)	404 (48)
Luminal B HER2-	93 (41, 35-47)	127 (56, 49-62)	61 (27, 21-33)	36 (16, 11-21)	22 (10, 6-14)	14 (6, 3-9)	227 (27)
Luminal B HER2+	24 (38, 26-49)	44 (69, 57-80)	13 (20, 10-30)	10 (16, 7-25)	4 (6, 3-12)	6 (9, 2-17)	64 (8)
HER2 type	28 (49, 36-62)	29 (51, 38-64)	4 (7, 0-14)	11 (19, 9-30)	6 (11, 2-19)	5 (9, 1-16)	57 (7)
Five negative	12 (40, 22-58)	14 (47, 28-65)	2 (7, 0-16)	3 (10, 0-21)	2 (7, 0-16)	1 (3, 0-10)	30 (4)
Basal	26 (43, 31-56)	19 (32, 20-44)	6 (10, 2-18)	11 (18, 8-28)	4 (7, 0-13)	7 (12, 3-20)	60 (7)
Number of breast cancer deaths	154	164	50	48	29	19	331
Age-adjusted HR (95% CI)[f]	1.12 (0.90-1.39)	1.04 (0.84-1.30)	0.98 (0.72-1.32)	1.24 (0.91-1.70)	1.61 (1.10-2.37)	0.92 (0.57-1.47)	-

Abbreviations: SD: standard deviation, CI: confidence interval, HR: hazard ratio.

[a] Negative: <1% positive tumor cells, positive: ≥1% positive tumor cells.

[b] Negative: staining index 0-2, positive: staining index ≥3.

[c] <10% and ≥10% granular cytoplasmic staining combined.

[d] Regardless of NPNT expression.

[e] Negative, but less than 5 nodes examined.

[f] Adjusted for age at diagnosis in 5-year categories; reference group is patients with negative staining pattern for the respective phenotype.

xCELLigence Adhesion and Migration Assay

The xCELLigence system (ACEA Biosciences Inc, San Diego, CA) was used for RTCA of adhesion and migration according to previous reports [22–25]. For adhesion assays E-plates (Cat.: 05469830001) were coated with recombinant mouse NPNT (Cat.: 4298-NP-050, R&D Systems, Minneapolis, NE) at 0.4, 2, or 10 μg/ml for 4 hours at 37°C prior to seeding. 66cl4- and 4T1-cell variants were detached from tissue culture vessels using 0.03% EDTA, spun and washed with serum-free medium, and seeded at either 20,000 or 40,000 cells/well, respectively, in serum-free medium. Adhesion was recorded by electrical impedance every 5 minutes for 24 hours. The arbitrary unit "cell index" is a measure of impedance, and the value is dependent on the number of cells, the size and shape of the cells, and the cell attachment quality. For the RGD peptide blocking experiments, E-plates were coated with 2 μg/ml recombinant mouse NPNT and blocked with 3% BSA for 1 hour at 37°C. The 66cl4-EV cells were detached with EDTA and seeded in serum-free medium containing a scrambled control peptide (Cat.: H-3166, H-Gly-Arg-Gly-Glu-Ser-OH Trifluoroacetate) or an RGD-blocking peptide (Cat.: H-1346, H-Gly-Arg-Gly-Asp-OH) at 0.5 mg/ml (Bachem, Bubendorf, Switzerland). Adhesion was analyzed at 9 hours after seeding. Migration was performed using xCELLigence CIM plates (Cat.: 05665825001) containing 160 μl medium with 10% serum in the lower chamber and 60,000 cells (66cl4 cell variants) in serum-free medium in the upper chamber. Wells containing serum-free medium in the lower chamber were included as controls. Cell index was recorded every 5 minutes.

Western Blot Analysis

Cells were lysed in 10 mM Tris-HCl buffer, and 30 μg of sample was run on a 10% Bis-Tris gel (Thermo Fisher Scientific, Waltham, MA). Proteins were transferred to PVDF membranes and incubated with anti-V5 (CST, Danvers, MA) (1:1000), anti-ALIX (CST, Cat.: 13202S, Lot No.: 2, dilution 1:1000), anti-CHMP4B (Atlas Antibodies/Sigma, Cat.: HPA051751, Lot No.: R67106, dilution1:500), and anti-GM130 (BD Biosciences, Cat.: 610822, Lot No.: 7069938, dilution 1:500). Equal loading was confirmed using anti-GAPDH (Abcam, Cat.: ab9484, Lot No.: GR165366-3, dilution 1:5000), and antibody binding was detected using HRP-linked secondary antibodies according to manufacturer's instructions (Dako). Full length blots are shown in Supplementary Figure S3.

Soft Agar Colony Assay

A bottom layer of 0.75% agarose in α-MEM and a top layer of 0.36% agarose/α-MEM mixed with 2000 cells/well were added to each well in 12-well plates. The cells were fed with normal growth medium and left for about 2 weeks with 2-3 medium replacements. Plates were stained with 0.005% crystal violet in 2% ethanol/PBS and colonies counted from triplicate wells per cell line.

Minimal Seeding Colony Assay

Cells were seeded onto plastic (10 cells/well in 12-well plates) and left for 10 days. Medium was replaced twice during the experiment, and the cells were fixed with 6% glutaraldehyde for 30 minutes and stained with 0.1% crystal violet for 30 minutes before rigorous washing with water. Colonies were counted from triplicate wells/cell line.

Proliferation Assay

A total of 1.3×10^6 cells were seeded in 25-cm^2 flasks and counted after 24, 48, and 72 hours with triplicate measurements per condition.

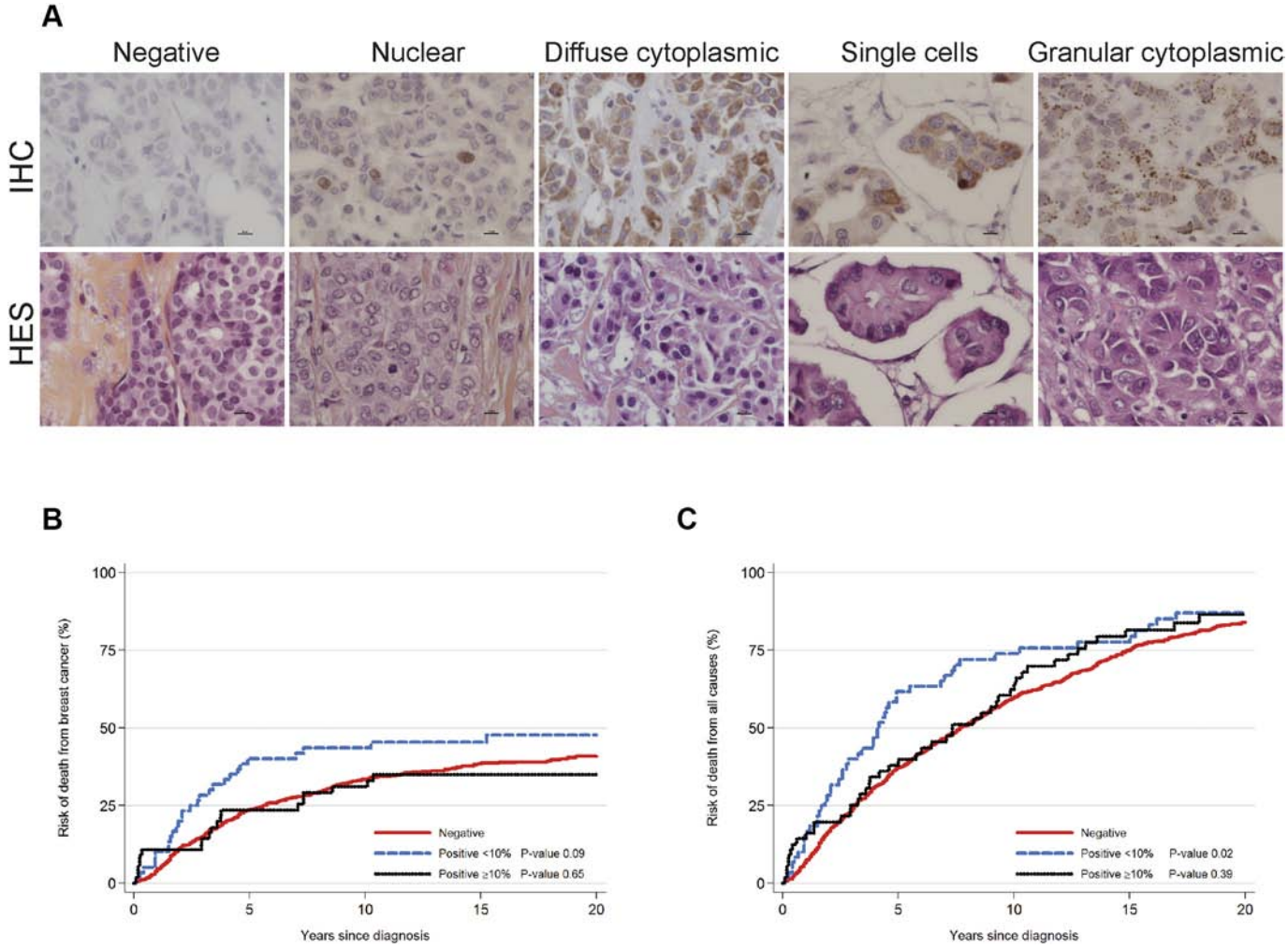

Figure 1. Granular NPNT staining patterns are associated with poor outcome in breast cancer patients. Representative images of IHC- and HES-stained TMA samples showing (A) different staining patterns: no staining, nuclear staining, diffuse cytoplasmic staining, and single cells positive or granular cytoplasmic staining using antibodies towards human NPNT (Atlas Antibodies/Sigma) imaged at 600× magnification. The images show representative cases of each staining phenotype, and the cases shown are Luminal A, Luminal A, Luminal B (HER2−), Luminal A and Luminal B (HER2−), respectively. Scale bars: 50 μm. Survival analysis showing association between no granular cytoplasmic staining (red line), 1-10% granular positive cells (thick dotted blue line), or >10% granular positive cells (solid black line) on (B) cumulative risk of death from breast cancer and (C) overall survival for all 842 patients represented in the TMAs.

RNA Scope ISH

ISH for NPNT mRNA was performed on the same mouse mammary biopsies from the transgenic MMTV-PyMT mice as the IHC staining. Custom-made probes (Mm-AF397008) and RNAscope®2.0 kit (Advanced Cell Diagnostics, Hayward, CA) were used according to the manufacturer's protocol.

Purification and Characterization of Microvesicles and Exosomes

Microvesicles and exosomes were purified using a standardized sequential ultracentrifugation protocol as described by Peinado et al. [26]. Cells were grown in 10% exosome-depleted FCS for 3 days and the cell culture supernatant harvested by centrifugation at 500*g* for 10 minutes. The microvesicle fraction (pellet) was collected by spinning at 12,000*g* for 20 minutes. Finally, the exosome fraction was collected by spinning at 100,000*g* for 70 minutes. Exosomes were washed in 20 ml PBS and pelleted again by ultracentrifugation (Beckman 70Ti rotor). Particle number of isolated microvesicles and exosomes was analyzed using the LM10-HS nanoparticle characterization system (NanoSight, Malvern Instruments Ltd, UK).

Statistical Analyses

We estimated risk of death from breast cancer according to NPNT expression, calculating cumulative incidence and with death from other causes as competing events. Risk of death from any cause was estimated using the Kaplan-Meier method. Equality between curves was assessed using Gray's test and the log-rank test, respectively. We used Cox proportional hazards models to estimate risk of death from breast cancer (censoring at death from other causes) calculating hazard ratios (HRs) with 95% confidence intervals (CIs) and adjusting for age, stage, grade, and subtype. *In vitro* experiments were evaluated in linear regression models. Indicators for each experiment were included to adjust for variation across experiments. In the animal experiments, groups were compared using two-tailed *t* tests.

Results

We showed previously that NPNT can function as a prometastatic protein in mouse breast cancer models [15]. With a well-characterized set of formalin-fixed and paraffin-embedded (FFPE) tumor samples from 842 Norwegian women diagnosed

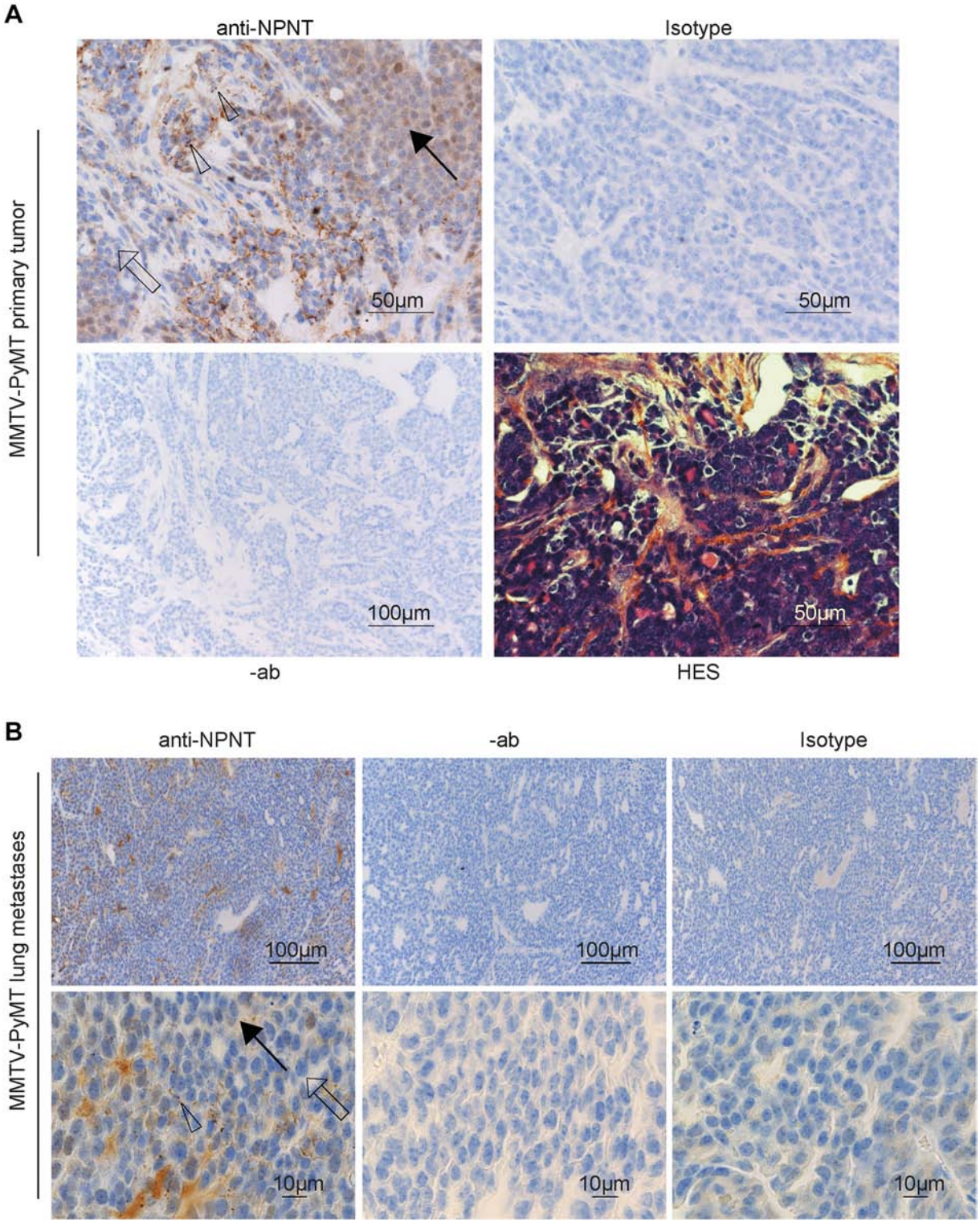

Figure 2. Phenotypically different patterns of NPNT staining in MMTV-PyMT transgenic mouse tumors. (A) Representative images of IHC- and HES-stained MMTV-PyMT primary tumors. NPNT was detected using antibodies towards mouse NPNT (Atlas Antibodies/Sigma). Figure shows antibody-stained sections, IgG Isotype control, control without antibodies (-ab), and HES-stained section from the same region. (B) Representative images of IHC-stained MMTV-PyMT lung metastases. Arrows indicate no staining (open arrow), diffuse cytoplasmic staining (filled arrow), and granular staining (triangle). Images are representative of a series of samples from nine mice.

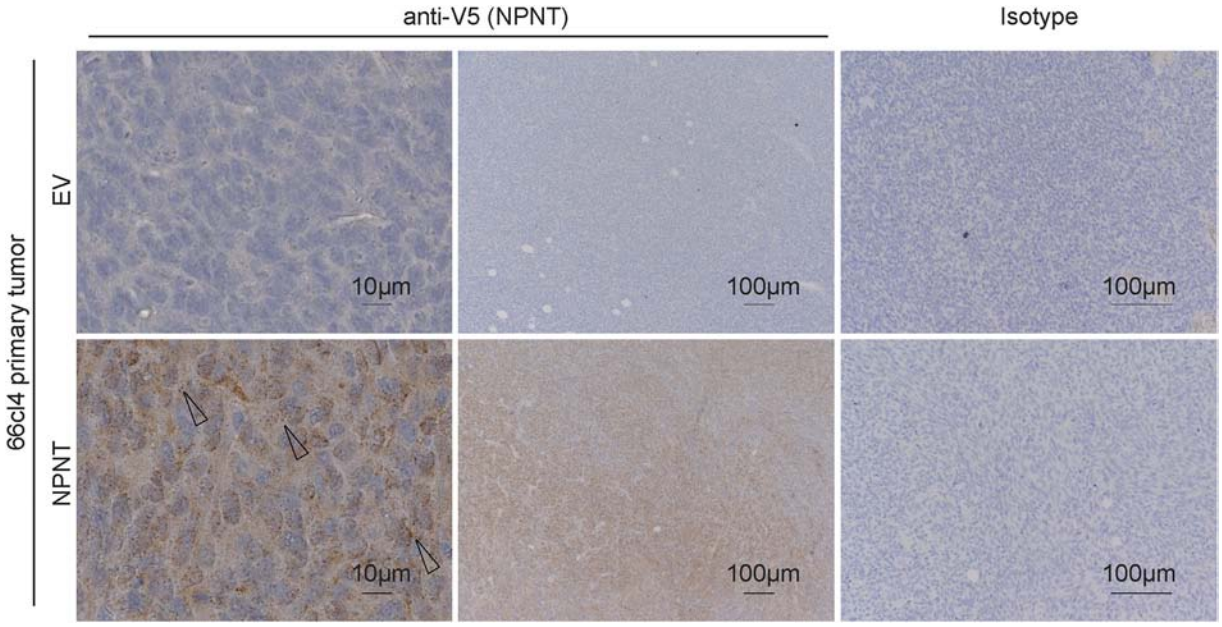

Figure 3. NPNT is located in granules in 66cl4-NPNT primary tumors. Representative images of IHC-stained 66cl4-EV and 66cl4-NPNT primary tumors using V5-specific antibodies (Cell Signaling Technology). The left and middle panels show antibody-stained sections, whereas the right panels show rabbit IgG Isotype staining controls. Granular staining is indicated with open triangles. Images are representative of a series of samples from five mice.

with invasive breast cancer between 1961 and 2008, [17] we assessed NPNT protein expression using IHC on TMAs. Using a standardized protocol developed for this study, we found positive NPNT staining in 596 out of 842 cases (70.8%). Interestingly, although NPNT has been shown previously to be an extracellular matrix protein, [8–10] in this study, we identified intracellular staining that we grouped into four different patterns: nuclear staining; diffuse positive cytoplasmic staining; scattered single cells with strong cytoplasmic staining and granular cytoplasmic staining (Table 1 and Figure 1*A*). Patients with 1-10% granular staining had a poorer prognosis than those with no granular staining, evaluating both risk of death from breast cancer (age-adjusted hazard ratio (HR) 1.61, 95% confidence interval (CI) 1.10-2.37, Table 1) and overall survival (Figure 1, *B* and *C*). In contrast, reduced survival was not found among patients with high (≥10%) granular NPNT staining (HR 0.92, 95% CI 0.57-1.47). In separate analyses of the different molecular subtypes, the association between the presence of any NPNT granular staining and prognosis was strongest for the Luminal A subtype (HR 1.70, 95% CI 0.99-2.90, *P*=.054) (Supplementary Table S1). The remaining staining patterns showed no significant association with prognosis. Adjustment for tumor stage and grade at diagnosis had little influence on the estimates. Taken together, this comprehensive analysis demonstrates for the first time that NPNT is localized intracellularly in a large number of human breast tumors and that low levels of intracellular granular staining may be associated with poor prognosis.

To investigate the presence and appearance of NPNT distribution in mouse breast tumors, we utilized a well-established transgenic mouse model of breast cancer, the MMTV-PyMT model [21,27]. NPNT was expressed at higher levels in isolated primary tumor cells compared to normal primary mammary epithelial cells from wild-type animals (Supplementary Figure S4*A*), and ISH analyses also confirmed that NPNT is exclusively expressed by the tumor cells (Supplementary Figure S4*B*). NPNT protein was present in the tumor cells, with phenotypically different patterns including diffuse cytoplasmic or granular cytoplasmic distribution (Figure 2*A*). Protein localization was tumor-cell-specific with limited staining in the extratumoral stromal tissue. Approximately 10% of the tumor cells had a granular staining pattern of NPNT similar to that found in the human tumors. The granular NPNT staining pattern has also been shown to be present in mouse tibias [28]. Direct comparison between NPNT and the ECM-proteins Collagen V and Fibronectin in ECM-rich areas of MMTV-PyMT tumors showed some signs of extracellular presence of NPNT; however, this was not the major site of localization (Supplementary Figure S2*B*). We investigated NPNT expression patterns in metastases in lung tissue from the MMTV-PyMT animals and found that the tumor cells were diffusely positive in the cytoplasm in the tumor periphery with a few granular-positive tumor cells similar to that of the primary tumors (Figure 2*B*). Taken together, these findings identify MMTV-PyMT–driven tumors as a potential model for further studies on the role of granular NPNT in breast cancer progression and metastasis.

To investigate the *in vivo* function of NPNT, we expressed a V5-tagged NPNT construct in weakly metastatic mouse 66cl4 breast cancer cells that express low endogenous levels of NPNT. End-stage orthotopic tumors were then stained by IHC using an anti-V5 antibody. The 66cl4-NPNT primary tumors revealed both diffuse and granular cytoplasmic NPNT staining similar to the human and MMTV-PyMT tumors (Figure 3). Consistent with our previous finding that reducing the initially high levels of NPNT in the highly metastatic cell line 4T1.2 does not affect primary tumor growth [15], there were no significant differences in tumor volume or weight at endpoint between the 66cl4-NPNT and 66cl4-EV tumors (Supplementary Figure S5, *A* and *B*). Measurement of RTB in spine and

lung [15] showed that increased NPNT expression was not sufficient to promote spontaneous metastasis of 66cl4 mammary tumors (Supplementary Figure S5, *C* and *D*). Taken together, these findings demonstrated that the NPNT staining patterns in the human samples could also be observed in the mouse tumors. We suggest that NPNT may be more important for metastatic dissemination than primary tumor growth.

Transcript levels of NPNT are correlated with the metastatic propensity of cells in the 4T1 model, with negligible levels in the low and weakly metastatic 67NR, 168FARN, and 66cl4 cells and higher levels in the more metastatic 4TO7 and 4T1 cells (Supplementary Figure S6*A*). Similarly, IHC staining of orthotopic primary tumors showed some weak cytoplasmic NPNT staining in 67NR tumors and slightly stronger NPNT staining in patches in 4T1 tumors

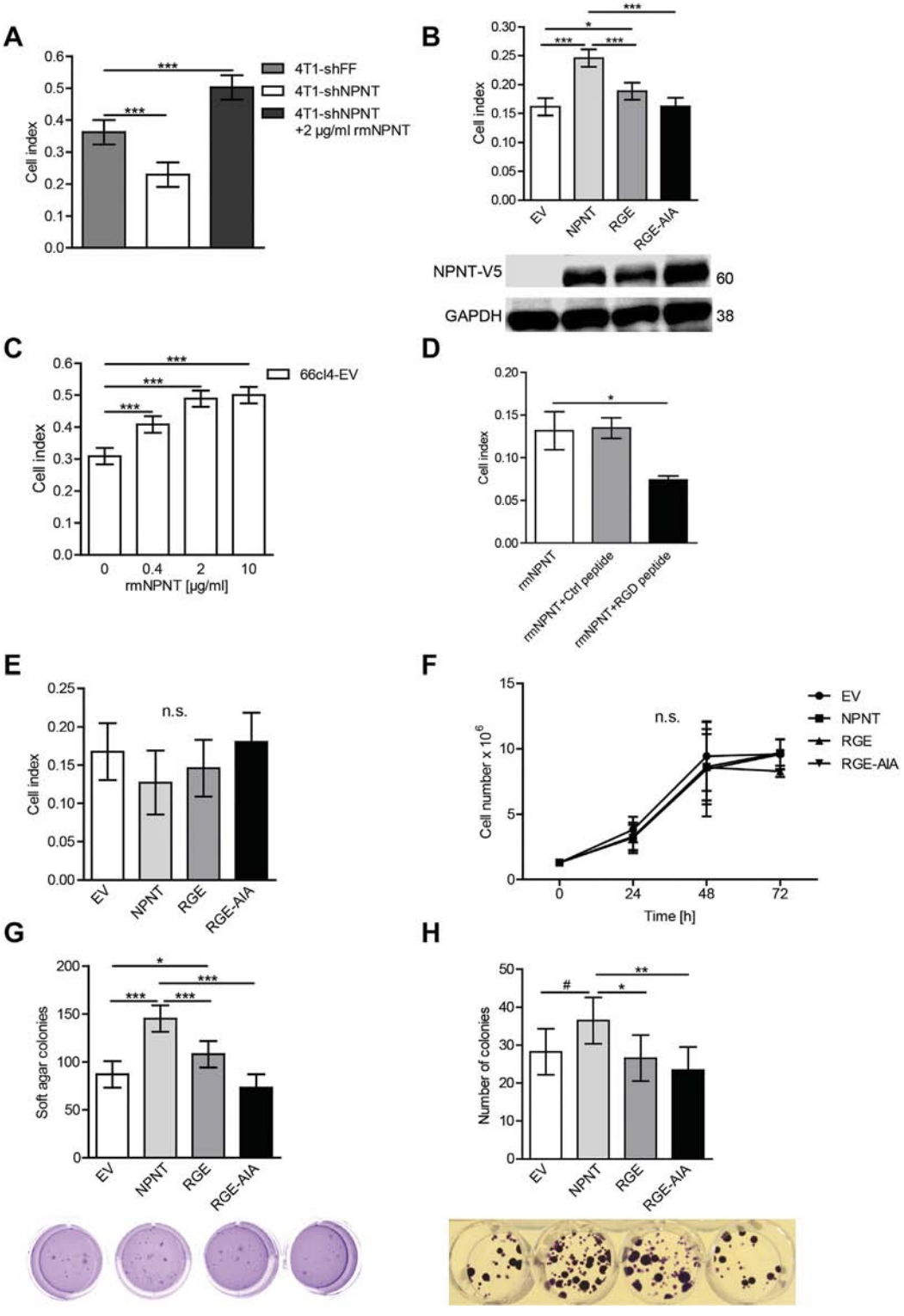

(Supplementary Figure S6*B*). Granular NPNT staining was not observed in these tissue samples. Using 4T1 cells with high endogenous NPNT levels, we created clones with stable knockdown of NPNT using shRNAs (Supplementary Figure S6*C*). The 4T1-shNPNT cell line displayed a significantly reduced ability to attach to uncoated wells compared to the 4T1-shFF (control) cells, but adhesion could be rescued by addition of 2 μg/ml recombinant mouse NPNT (rmNPNT) (Figure 4*A*). The 4T1-shFF and 4T1-shNPNT lines both showed a dose-dependent increase in adhesion to rmNPNT-coated plates 1 hour after seeding (Supplementary Figure S6*D*).

Previous research has demonstrated that binding of NPNT to its receptor integrin α8β1 is mediated through both the high-affinity RGD sequence and an additional downstream enhancer site (EIE) [29,30]. An adhesion assay of 66cl4 cells with enhanced expression of either native NPNT or NPNT mutants (RGE or RGE-AIA) showed that while exogenous NPNT enhanced adhesion, disruption of the RGD-site alone or of both the RGD and the EIE sites significantly reduced adhesion (Figure 4*B*). Increased NPNT protein expression was confirmed by Western blot. The 66cl4-EV cells showed a dose-dependent increase in adhesion to plates coated with rmNPNT (Figure 4*C*), and this adhesion was reduced in the presence of a RGD-blocking peptide, demonstrating the involvement of RGD-binding integrins (Figure 4*D*). There was no impact on either migration or proliferation upon NPNT overexpression (Figure 4, *E* and *F*). A soft agar colony forming assay showed that the 66cl4-NPNT cells exhibited a significantly increased capacity to grow in an anchorage-independent manner (Figure 4*G*). This increase was abolished when both RGD and EIE were mutated. Furthermore, using a minimal density seeding assay with 10 cells per well, we observed that cells expressing NPNT had a tendency towards increased ability to grow colonies from single cells (P=.064) (Figure 4*H*). Again, this increase was reduced when both RGD and EIE were mutated. Taken together, these *in vitro* assays indicate that NPNT is involved in adhesion and anchorage-independent growth, implying a role for NPNT in colony formation at the secondary site.

The 66cl4 tumor has low spontaneous metastatic capacity, and we have found that expression of NPNT is not sufficient to increase spontaneous metastasis. However, it is possible that NPNT can influence the ability of tumor cells to lodge in the lung and grow into metastatic lesions. To address this, we inoculated mice with tumor cells via the tail vein and measured subsequent colonization of the lung. We found that NPNT does promote lung colonization and that this is mediated via the RGD and EIE sites as shown by both the increased lung weight and lung tumor burden in mice injected with cells expressing wild-type NPNT compared to the empty vector (EV) cells (Figure 5*A* and *B*). There was no significant difference between cells expressing wild-type NPNT and the RGE mutant, but the increased colonization capability was completely abolished in the double mutant, demonstrating the importance of the enhancer EIE site in the ability to colonize the lung. Images of representative lungs from each group show that the increased lung weight (Figure 5*A*) and relative tumor burden (RTB, Figure 5*B*) were caused by an increased number of metastatic lesions and not just an increase in size of the colonies (Figure 5*C*). In summary, this experimental metastasis assay showed that NPNT promotes lung colonization via the enhancer (EIE) sites, possibly aided by the RGD motif, and confirms an *in vivo* effect of the two motifs responsible for integrin interaction. IHC staining of lung metastases from the lung colonization assay showed that also the tumor cells in the metastatic lesions displayed a granular pattern of NPNT staining (Figure 5*D*).

Cancer cell extracellular vesicles and their role in angiogenesis, tumor progression, and metastasis is of increasing interest in cancer research [31–33], and NPNT has been detected previously in proteomic characterizations of isolated exosomes from human ductal saliva and colorectal cancer cells [34,35]. The granular staining patterns observed in the human samples, MMTV-PyMT tissues, 66cl4-NPNT primary tumors, and metastases prompted us to speculate that these granular structures could be multivesicular bodies containing exosomes. To address this, we isolated both exosomes and microvesicles from 66cl4-NPNT cells using well-established protocols [26]. ALIX and CHMP4B are commonly used markers for exosome-containing multivesicular bodies [35–37]. By Western blot, we show that NPNT co-purified with ALIX and CHMP4B in extracellular vesicles released from cells expressing both wild-type and mutant NPNT (Figure 6*A*), hinting that the localization of NPNT to microvesicles and exosomes is not integrin-dependent. In accordance with the recommended guidelines for extracellular vesicle characterization [38], we

Figure 4. NPNT increases adhesion and anchorage-independent growth. (A) Adhesion of 4T1-shFF and 4T1-shNPNT cells in an xCELLigence adhesion assay. The figure shows rescue of adhesion in 4T1-shNPNT cells in plates coated with 2 μg/ml recombinant mouse NPNT (rmNPNT). 4T1-shFF cells express a nontargeting control shRNA. Data are presented as mean cell index ± 95% CI from two experiments (n=4), 1 hour after seeding. (B) xCELLigence adhesion assay of 66cl4-cells expressing either EV or NPNT wild-type, NPNT RGE, or NPNT RGE-AIA mutants in uncoated plates. Data are presented as mean cell index ± 95%CI from four experiments (n=3-12), 1 hour after seeding. Lower panel shows Western blot of cell lysates confirming NPNT overexpression detected with the anti-V5 antibody. The image is cropped to display only relevant bands, but the full blot is shown in Supplementary Figure S3*A*. (C) Adhesion assay of 66cl4-EV cells in plates coated with rmNPNT at 0.4 μg/ml, 2 μg/ml, or 10 μg/ml prior to seeding. Data are presented as mean cell index ± 95% CI from two experiments (n=4), 1 hour after seeding. (D) Adhesion assay of 66cl4-EV cells in rmNPNT-coated wells in presence of either scrambled peptide or RGD-blocking peptide. Data are presented as mean cell index±SEM from three experiments with n=2 in each experiment. (E) Migration assay in xCELLigence CIM-plates using 66cl4-cells expressing either EV or NPNT wild-type, NPNT RGE, or NPNT RGE-AIA mutants. Migration towards 10% FCS was recorded every 5 minutes, and data are presented as mean cell index ± 95%CI at 12 hours from 5 individual experiments with n=2-4 technical replicates in each experiment. (F) Cell proliferation assay with 1.3×10^6 cells per 25-cm^2 flask. Cells were harvested and counted after 24, 48, and 72 hours, and data are shown as mean ± SD from three individual experiments. (G) Soft agar assay for anchorage-independent growth of 66cl4-cells expressing EV, NPNT, NPNT RGE, or NPNT RGE-AIA. Two thousand cells/well in 12-well plates were seeded in 0.36% agarose/α-MEM medium containing 10% FCS and grown for 10 days. Data presented as mean ± 95% CI from 3 individual experiments (n=3-9). (H) Clonogenic cell survival assay with minimal seeding density of 66cl4-cells expressing EV, NPNT, NPNT RGE, or NPNT RGE-AIA. A total of 10 cells/well were seeded in 12-well plates and grown as single colonies for 10 days. Graph shows number of colonies as mean ±95% CI from five individual experiments with n=3-9 replicates per experiment. # indicates P=.064 when comparing EV-cells with NPNT-expressing cells. All *in vitro* data except the qRT-PCR and the proliferation assay were analyzed with linear regression models. ***P<.0001, **P<.005, *P<.05.

show that the isolated vesicles were negative for the Golgi marker GM130. Immunofluorescence staining of 66cl4-NPNT lung metastases and MMTV-PyMT tumor tissues confirmed colocalization of NPNT with CHMP4B, leading us to propose that the cytoplasmic granular structures could be NPNT-containing multivesicular bodies (Figure 6, *B* and *C*). In conclusion, we have demonstrated that NPNT is present in extracellular vesicles and that NPNT facilitates colonization at the metastatic site via its integrin-binding sites.

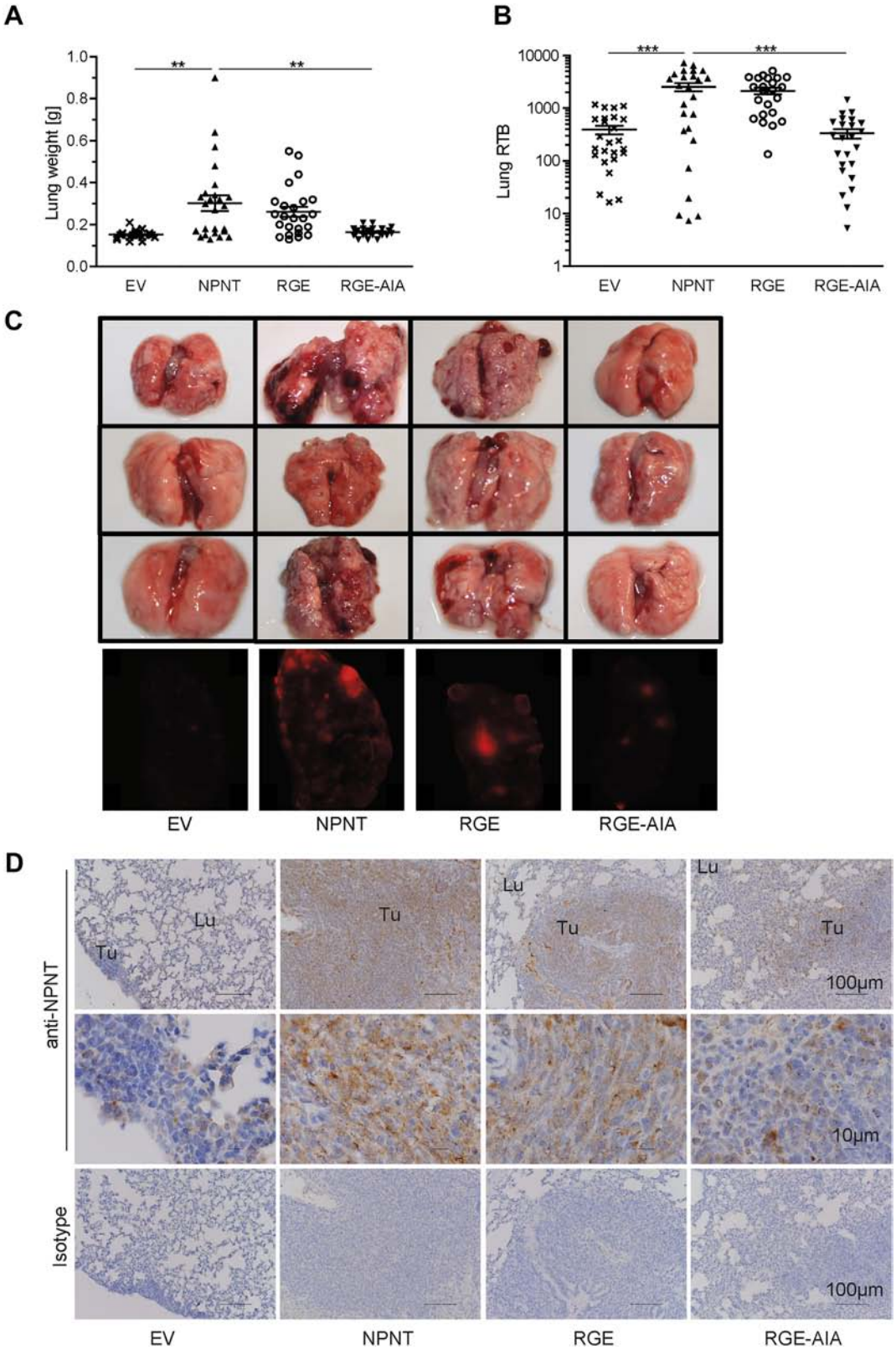

Discussion

We found positive NPNT staining in the majority of patient samples (70.8%), demonstrating that NPNT is present in human breast tumors. Although NPNT has been shown by others to be an extracellular matrix protein, we found that it is also localized intracellularly in tumor cells. Interestingly, in our patients' tumors, granular intracellular staining in less than 10% of the cells was associated with decreased survival. In addition, we showed the presence of several phenotypically different intracellular staining patterns, including diffuse cytoplasmic and nuclear NPNT staining; however, neither of these was correlated with survival. This may reflect a preference of the antibody to recognize the core protein and not the highly glycosylated secreted forms of the protein when analyzed by IHC.

We did not observe any association between granular NPNT staining and lymph node metastasis in our patient samples. The total number of cases with known metastases was 297. However, lymph node status was not reported in 215 (25.5%) cases, and the granular staining pattern was observed in only 116 (13.8%) cases. Our analyses showed an association between granular staining patterns (<10% positive tumor cells) and poor outcome in patients with luminal A subtype (P=.054), but since numbers were lower for the other subtypes, statistical power was limited in these subgroups.

The nonlinear U-shaped correlation between granular cytoplasmic staining of NPNT and survival is similar to that shown for various tumor markers in glioma [39], prostate [40,41], colorectal [42,43], and pancreatic cancer [44,45]. In addition, a recent study reported a U-shaped correlation between HER2 protein expression and overall survival of breast cancer patients treated with the tyrosine kinase inhibitor lapatinib [46]. The explanation for this phenomenon is unclear in most cases. Similarly, we identified nuclear staining of NPNT in a proportion of the patient samples. This has also been reported in human MCF-7 breast cancer cells on the Human Protein Atlas website available from www.proteinatlas.org [47]. The possible function of NPNT in the nucleus is unknown and should be followed up in future studies. Taken together, this is the first extensive characterization of NPNT expression in a large cohort of breast cancer patients, and although the results need to be verified by similar studies of other cohorts, they warrant further investigation into the role of NPNT in breast cancer.

We have shown previously that reduced NPNT expression in the highly metastatic 4T1.2 cells caused a significant reduction in metastatic tumor burden in lung, spine, and kidneys, [15], and in the present study, we show that enhanced expression of NPNT in low-metastatic 66cl4 cells increased the colonization capacity in the lungs. Our lung colonization data clearly demonstrated that 66cl4 cells expressing NPNT have a significantly increased capability to seed and grow in the lungs in an integrin-dependent manner. Our results are supported by findings from Sánches-Cortés et al. showing that the RGD and the FEI or EIE sites function synergistically and are both important for the interaction between NPNT and its integrin receptor [29]. Previous reports showed that the main receptor for NPNT is integrin α8β1 [8,10]. However, we cannot exclude the possibility that NPNT might also interact with other receptors, for example, integrin αVβ3, on the lung endothelium during the metastatic process [19]. Our findings will prompt further studies on the role of NPNT in breast cancer using experimental models. The IHC of the MMTV-PyMT tissues revealed staining patterns similar to those in human cancers, suggesting that this might be a suitable model for further studies.

NPNT has been shown previously to be involved in breast cancer metastasis in mice [15,16]. Although we were unable to show a link between NPNT expression and metastasis in our patient material, the results from the experimental models showed that tumor cells expressing NPNT were more prone to establish colonies in lungs and to display increased adhesion and anchorage-independent growth *in vitro* in an integrin-dependent manner.

The role of extracellular vesicles in tumor progression and metastasis is an emerging topic in cancer research, and exosomes have been shown to facilitate increased proliferation, evasion of apoptosis, stimulation of migration, invasion, and metastasis in addition to resistance to therapy (reviewed in [48–51]). Furthermore, the packaging of exosomal content is likely to be specific since the exosomal content influences organotropic dissemination [52]. The data presented here suggest for the first time that NPNT may be localized in mouse breast cancer cell–derived exosomes, and our *in vivo* data revealed that there might be a link between NPNT-containing exosomes and increased metastatic capacity.

In conclusion, NPNT was originally described as an extracellular matrix protein [8,10], but the findings from mouse tumor tissues presented here show intracellular NPNT staining in primary tumors both diffusely in the cytoplasm and in exosome-containing multivesicular bodies. We found that granular intracellular staining in less than 10 % of tumor cells was associated with decreased survival in a large cohort of breast cancer patients and that the integrin-binding site was important for lung colonization of 66cl4 cells in our animal model. There are clearly several mechanisms of action for NPNT in promoting breast cancer, warranting further investigation into NPNT as a potential prognostic marker and a possible future target for therapy in a subgroup of breast cancer patients.

Supplementary data to this article can be found online at https://doi.org/10.1016/j.neo.2018.02.008.

Acknowledgements and Funding

The mouse cell lines 67NR, 168FARN, 66cl4, 4TO7, and 4T1 were kindly provided by Dr. Fred Miller. We thank Dr. Naoko Morimura

Figure 5. NPNT promotes colonization of the lung via its integrin-binding motifs. 66cl4-cells expressing EV, NPNT wild-type, NPNT RGE, or NPNT RGE-AIA mutants were injected into the lateral tail vein to assess tumor cell colonization of the lung using 24-25 mice per group. (A) Lungs were collected after 3 weeks and weighed (mean±SD). $^{**}P<.0005$ when analyzed by two-tailed t test. The data have been merged from two separate experiments using 14-15 and 9-10 mice per group. (B) RTB assay using genomic DNA from whole lung lysates as template (n=24-25). Graphs show mean RTB ± SD, $^{***}P<.0001$ when analyzed by two-tailed t-test. (C) Images of three representative lungs from each group of mice. Macroscopic view of representative lung lobes imaged to detect mCherry positive tumor cells (bottom row). The tissues were imaged using the EVOS FL Auto Cell Imaging System with an inverted microscope and a Sony ICX445 monochrome CCD camera and visualized using 4× objectives. Each image was created using a stitch of several images to cover the entire lung lobe. (D) Representative images of IHC-stained lungs from mice using NPNT antibodies (Atlas Antibodies/Sigma). The top and middle rows show antibody-stained sections at two different magnifications, whereas the lower row shows rabbit IgG isotype staining controls. Scale bars: top and lower row: 100 μm, middle row: 10 μm. Tu: indicates tumor area, Lu: indicates normal lung tissue. Images are representative of a series of samples from five mice.

for the pcDNA3-POEM-Fc vector. We thank Knut Sverre Grøn, Shalini Vasudev Rao, and Ulrike Neckmann for skillful technical assistance with animal experiments; Borgny Ytterhus, Bjørn Munkvold, and Negar Shahini for valuable help with histology; and Hector Peinado, Lucia Robado de Lope, and Marta Hergueta-Redondo for collaboration regarding exosome isolation protocols. The study received funding from the Research Council of Norway [grant number 197282], The Liaison Committee between

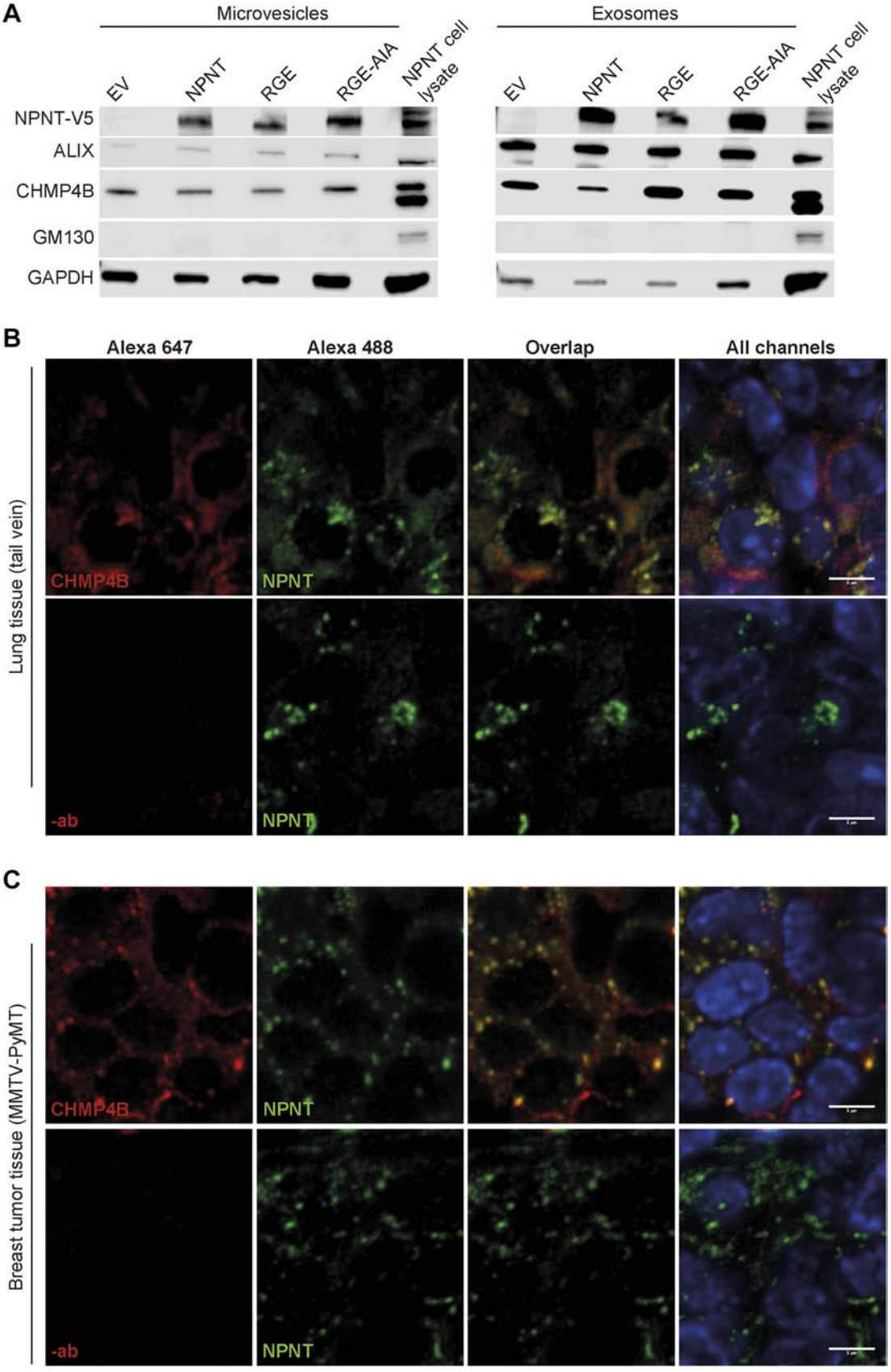

the Central Norway Regional Health Authority and the Norwegian University of Science and Technology (NTNU) [grant numbers 46056732, 46055600, and 46077600], the Cancer Fund at St. Olav's Hospital in Trondheim, The Northern Norway Regional Health Authority (Helse Nord RHF), UiT-The Arctic University of Norway [grant number SFP1232-15], and The National Cancer Institute at NIH. We acknowledge fellowships from the National Breast Cancer Foundation of Australia to Richard Redvers and Robin Anderson. The Research Council of Norway is acknowledged for the support to the Norwegian Micro- and Nano-Fabrication Facility, NorFab [grant number 245963/F50].

Author contributions

T.S.S., R.O.H., R.L.A., and G.S. conceived the project. T.S.S., J.T., R.P.R., A.M.B., R.L.A., and G.S. designed the experiments. T.S.S., J.T., R.P.R., S.N.M., B.L.E., J.M.L., J.D., and G.S. conducted experiments. T.S.S., J.T., M.V., A.M.B., S.O., S.L., and G.S. performed data analysis. T.S.S., M.V., S.N.M., A.M.B., R.O.H, R.L.A., and G.S. wrote and critically appraised the manuscript. All authors have read and revised the manuscript.

Conflicts of Interest

The authors declare that they have no competing interests.

References

[1] Jemal A, Bray F, Center MM, Ferlay J, Ward E, and Forman D (2011). Global cancer statistics. *CA Cancer J Clin* **61**, 69–90.

[2] Kast K, Link T, Friedrich K, Petzold A, Niedostatek A, Schoffer O, Werner C, Klug SJ, Werner A, and Gatzweiler A, et al (2015). Impact of breast cancer subtypes and patterns of metastasis on outcome. *Breast Cancer Res Treat* **150**, 621–629.

[3] Chambers AF, Groom AC, and MacDonald IC (2002). Dissemination and growth of cancer cells in metastatic sites. *Nat Rev* **2**, 563–572.

[4] Toss A and Cristofanilli M (2015). Molecular characterization and targeted therapeutic approaches in breast cancer. *Breast Cancer Res* **17**, 60.

[5] Perou CM, Sorlie T, Eisen MB, van de Rijn M, Jeffrey SS, Rees CA, Pollack JR, Ross DT, Johnsen H, and Akslen LA, et al (2000). Molecular portraits of human breast tumours. *Nature* **406**, 747–752.

[6] Sorlie T, Perou CM, Tibshirani R, Aas T, Geisler S, Johnsen H, Hastie T, Eisen MB, van de Rijn M, and Jeffrey SS, et al (2001). Gene expression patterns of breast carcinomas distinguish tumor subclasses with clinical implications. *Proc Natl Acad Sci U S A* **98**, 10869–10874.

[7] Esposito A, Criscitiello C, and Curigliano G (2015). Highlights from the 14(th) St Gallen International Breast Cancer Conference 2015 in Vienna: dealing with classification, prognostication, and prediction refinement to personalize the treatment of patients with early breast cancer. *Ecancermedicalscience* **9**, 518.

[8] Brandenberger R, Schmidt A, Linton J, Wang D, Backus C, Denda S, Muller U, and Reichardt LF (2001). Identification and characterization of a novel extracellular matrix protein nephronectin that is associated with integrin alpha8beta1 in the embryonic kidney. *J Cell Biol* **154**, 447–458.

[9] Linton JM, Martin GR, and Reichardt LF (2007). The ECM protein nephronectin promotes kidney development via integrin alpha8beta1-mediated stimulation of Gdnf expression. *Development* **134**, 2501–2509.

[10] Morimura N, Tezuka Y, Watanabe N, Yasuda M, Miyatani S, Hozumi N, and Tezuka Ki K (2001). Molecular cloning of POEM: a novel adhesion molecule that interacts with alpha8beta1 integrin. *J Biol Chem* **276**, 42172–42181.

[11] Fujiwara H, Ferreira M, Donati G, Marciano DK, Linton JM, Sato Y, Hartner A, Sekiguchi K, Reichardt LF, and Watt FM (2011). The basement membrane of hair follicle stem cells is a muscle cell niche. *Cell* **144**, 577–589.

[12] Toyoshima KE, Asakawa K, Ishibashi N, Toki H, Ogawa M, Hasegawa T, Irie T, Tachikawa T, Sato A, and Takeda A, et al (2012). Fully functional hair follicle regeneration through the rearrangement of stem cells and their niches. *Nat Commun* **3**, 784.

[13] Patra C, Diehl F, Ferrazzi F, van Amerongen MJ, Novoyatleva T, Schaefer L, Muhlfeld C, Jungblut B, and Engel FB (2011). Nephronectin regulates atrioventricular canal differentiation via Bmp4-Has2 signaling in zebrafish. *Development* **138**, 4499–4509.

[14] Patra C, Ricciardi F, and Engel FB (2012). The functional properties of nephronectin: an adhesion molecule for cardiac tissue engineering. *Biomaterials* **33**, 4327–4335.

[15] Eckhardt BL, Parker BS, van Laar RK, Restall CM, Natoli AL, Tavaria MD, Stanley KL, Sloan EK, Moseley JM, and Anderson RL (2005). Genomic analysis of a spontaneous model of breast cancer metastasis to bone reveals a role for the extracellular matrix. *Mol Cancer Res* **3**, 1–13.

[16] Borowsky AD, Namba R, Young LJ, Hunter KW, Hodgson JG, Tepper CG, McGoldrick ET, Muller WJ, Cardiff RD, and Gregg JP (2005). Syngeneic mouse mammary carcinoma cell lines: two closely related cell lines with divergent metastatic behavior. *Clin Exp Metastasis* **22**, 47–59.

[17] Engstrom MJ, Opdahl S, Hagen AI, Romundstad PR, Akslen LA, Haugen OA, Vatten LJ, and Bofin AM (2013). Molecular subtypes, histopathological grade and survival in a historic cohort of breast cancer patients. *Breast Cancer Res Treat* **140**, 463–473.

[18] Aslakson CJ and Miller FR (1992). Selective events in the metastatic process defined by analysis of the sequential dissemination of subpopulations of a mouse mammary tumor. *Cancer Res* **52**, 1399–1405.

[19] Sloan EK, Pouliot N, Stanley KL, Chia J, Moseley JM, Hards DK, and Anderson RL (2006). Tumor-specific expression of alphavbeta3 integrin promotes spontaneous metastasis of breast cancer to bone. *Breast Cancer Res* **8**, R20.

[20] Carter RZ, Micocci KC, Natoli A, Redvers RP, Paquet-Fifield S, Martin AC, Denoyer D, Ling X, Kim SH, and Tomasin R, et al (2015). Tumour but not stromal expression of beta3 integrin is essential, and is required early, for spontaneous dissemination of bone-metastatic breast cancer. *J Pathol* **235**, 760–772.

[21] Guy CT, Cardiff RD, and Muller WJ (1992). Induction of mammary tumors by expression of polyomavirus middle T oncogene: a transgenic mouse model for metastatic disease. *Mol Cell Biol* **12**, 954–961.

[22] Selvik LK, Rao S, Steigedal TS, Haltbakk I, Misund K, Bruland T, Prestvik WS, Laegreid A, and Thommesen L (2014). Salt-inducible kinase 1 (SIK1) is induced by gastrin and inhibits migration of gastric adenocarcinoma cells. *PLoS One* **9**e112485.

[23] Steigedal TS, Prestvik WS, Selvik LK, Fjeldbo CS, Bruland T, Laegreid A, and Thommesen L (2013). Gastrin-induced proliferation involves MEK partner 1 (MP1). *In Vitro Cell Dev Biol Anim* **49**, 162–169.

[24] Scrace S, O'Neill E, Hammond EM, and Pires IM (2013). Use of the xCELLigence system for real-time analysis of changes in cellular motility and adhesion in physiological conditions. *Methods Mol Biol* **1046**, 295–306.

[25] Hamidi H, Lilja J, and Ivaska J (2017). Using xCELLigence RTCA Instrument to Measure Cell Adhesion. *Bio Protoc* 7.

[26] Peinado H, Aleckovic M, Lavotshkin S, Matei I, Costa-Silva B, Moreno-Bueno G, Hergueta-Redondo M, Williams C, Garcia-Santos G, and Ghajar C, et al (2012). Melanoma exosomes educate bone marrow progenitor cells toward a pro-metastatic phenotype through MET. *Nat Med* **18**, 883–891.

Figure 6. NPNT is localized in extracellular vesicles. (A) Western blot of isolated microvesicles and exosomes from 66cl4-cells expressing EV, NPNT wild-type, NPNT RGE, or NPNT RGE-AIA detected with anti-V5 antibodies (CST). ALIX and CHMP4B were used as markers for microvesicles and exosomes, GM130 as a negative control and GAPDH for normalization control. Whole-cell lysates of 66cl4-NPNT cells were included as control. The images are cropped to display only relevant bands. Full-length blots are shown in Supplementary Figure S3. IF showing colocalization between the exosomal marker CHMP4B and NPNT detected with anti-CHMP4B and NPNT antibodies (Abnova) and visualized with Alexa Fluor 647 and Alexa Fluor 488 secondary antibodies, respectively, of (B) lung samples from *in vivo* lung colonization assay and (C) MMTV-PyMT mammary tumor samples. Images are representative of a series from five mice. Nuclei were stained with Hoechst. -ab reflects a control with no primary antibody. Scale bar; 5 μm

[27] Lin EY, Jones JG, Li P, Zhu L, Whitney KD, Muller WJ, and Pollard JW (2003). Progression to malignancy in the polyoma middle T oncoprotein mouse breast cancer model provides a reliable model for human diseases. *Am J Pathol* **163**, 2113–2126.

[28] Kuek V, Yang Z, Chim SM, Zhu S, Xu H, Chow ST, Tickner J, Rosen V, Erber W, and Li X, et al (2016). NPNT is expressed by osteoblasts and mediates angiogenesis via the activation of extracellular signal-regulated kinase. *Sci Rep* **6**, 36210.

[29] Sanchez-Cortes J and Mrksich M (2011). Using self-assembled monolayers to understand alpha8beta1-mediated cell adhesion to RGD and FEI motifs in nephronectin. *ACS Chem Biol* **6**, 1078–1086.

[30] Sato Y, Uemura T, Morimitsu K, Sato-Nishiuchi R, Manabe R, Takagi J, Yamada M, and Sekiguchi K (2009). Molecular basis of the recognition of nephronectin by integrin alpha8beta1. *J Biol Chem* **284**, 14524–14536.

[31] Azmi AS, Bao B, and Sarkar FH (2013). Exosomes in cancer development, metastasis, and drug resistance: a comprehensive review. *Cancer Metastasis Rev* **32**, 623–642.

[32] van der Pol E, Boing AN, Harrison P, Sturk A, and Nieuwland R (2012). Classification, functions, and clinical relevance of extracellular vesicles. *Pharmacol Rev* **64**, 676–705.

[33] Zomer A, Maynard C, Verweij FJ, Kamermans A, Schafer R, Beerling E, Schiffelers RM, de Wit E, Berenguer J, and Ellenbroek SI, et al (2015). In vivo imaging reveals extracellular vesicle-mediated phenocopying of metastatic behavior. *Cell* **161**, 1046–1057.

[34] Gonzalez-Begne M, Lu B, Han X, Hagen FK, Hand AR, Melvin JE, and Yates JR (2009). Proteomic analysis of human parotid gland exosomes by multidimensional protein identification technology (MudPIT). *J Proteome Res* **8**, 1304–1314.

[35] Demory Beckler M, Higginbotham JN, Franklin JL, Ham AJ, Halvey PJ, Imasuen IE, Whitwell C, Li M, Liebler DC, and Coffey RJ (2013). Proteomic analysis of exosomes from mutant KRAS colon cancer cells identifies intercellular transfer of mutant KRAS. *Mol Cell Proteomics* **12**, 343–355.

[36] Mathivanan S, Lim JW, Tauro BJ, Ji H, Moritz RL, and Simpson RJ (2010). Proteomics analysis of A33 immunoaffinity-purified exosomes released from the human colon tumor cell line LIM1215 reveals a tissue-specific protein signature. *Mol Cell Proteomics* **9**, 197–208.

[37] Willms E, Johansson HJ, Mager I, Lee Y, Blomberg KE, Sadik M, Alaarg A, Smith CI, Lehtio J, and El Andaloussi S, et al (2016). Cells release subpopulations of exosomes with distinct molecular and biological properties. *Sci Rep* **6**, 22519.

[38] Lotvall J, Hill AF, Hochberg F, Buzas EI, Di Vizio D, Gardiner C, Gho YS, Kurochkin IV, Mathivanan S, and Quesenberry P, et al (2014). Minimal experimental requirements for definition of extracellular vesicles and their functions: a position statement from the International Society for Extracellular Vesicles. *J Extracell Vesicles* **3**, 26913.

[39] Wang S, Chen Y, Qu F, He S, Huang X, Jiang H, Jin T, Wan S, and Xing J (2014). Association between leukocyte telomere length and glioma risk: a case-control study. *Neuro-Oncology* **16**, 505–512.

[40] Salonia A, Abdollah F, Capitanio U, Suardi N, Briganti A, Gallina A, Colombo R, Ferrari M, Castagna G, and Rigatti P, et al (2012). Serum sex steroids depict a nonlinear u-shaped association with high-risk prostate cancer at radical prostatectomy. *Clin Cancer Res* **18**, 3648–3657.

[41] Sandblom G, Ladjevardi S, Garmo H, and Varenhorst E (2008). The impact of prostate-specific antigen level at diagnosis on the relative survival of 28,531 men with localized carcinoma of the prostate. *Cancer* **112**, 813–819.

[42] Aleksandrova K, Chuang SC, Boeing H, Zuo H, Tell GS, Pischon T, Jenab M, Bueno-de-Mesquita B, Vollset SE, and Midttun O, et al (2015). A prospective study of the immune system activation biomarker neopterin and colorectal cancer risk. *J Natl Cancer Inst* **107**.

[43] Cui Y, Cai Q, Qu S, Chow WH, Wen W, Xiang YB, Wu J, Rothman N, Yang G, and Shu XO, et al (2012). Association of leukocyte telomere length with colorectal cancer risk: nested case-control findings from the Shanghai Women's Health Study. *Cancer Epidemiol Biomark Prev* **21**, 1807–1813.

[44] Chuang SC, Stolzenberg-Solomon R, Ueland PM, Vollset SE, Midttun O, Olsen A, Tjonneland A, Overvad K, Boutron-Ruault MC, and Morois S, et al (2011). A U-shaped relationship between plasma folate and pancreatic cancer risk in the European Prospective Investigation into Cancer and Nutrition. *Eur J Cancer* **47**, 1808–1816.

[45] Skinner HG, Gangnon RE, Litzelman K, Johnson RA, Chari ST, Petersen GM, and Boardman LA (2012). Telomere length and pancreatic cancer: a case-control study. *Cancer Epidemiol Biomark Prev* **21**, 2095–2100.

[46] Duchnowska R, Sperinde J, Czartoryska-Arlukowicz B, Mysliwiec P, Winslow J, Radecka B, Petropoulos C, Demlova R, Orlikowska M, and Kowalczyk A, et al (2017). Predictive value of quantitative HER2, HER3 and p95HER2 levels in HER2-positive advanced breast cancer patients treated with lapatinib following progression on trastuzumab. *Oncotarget* **8**, 104149–104159.

[47] Thul PJ, Akesson L, Wiking M, Mahdessian D, Geladaki A, Ait Blal H, Alm T, Asplund A, Bjork L, and Breckels LM, et al (2017). A subcellular map of the human proteome. *Science* 356.

[48] Wu CY, Du SL, Zhang J, Liang AL, and Liu YJ (2017). Exosomes and breast cancer: a comprehensive review of novel therapeutic strategies from diagnosis to treatment. *Cancer Gene Ther* **24**, 6–12.

[49] Lowry MC, Gallagher WM, and O'Driscoll L (2015). The role of exosomes in breast cancer. *Clin Chem* **61**, 1457–1465.

[50] Yu S, Cao H, Shen B, and Feng J (2015). Tumor-derived exosomes in cancer progression and treatment failure. *Oncotarget* **6**, 37151–37168.

[51] Villagrasa A, Alvarez PJ, Osuna A, Garrido JM, Aranega A, and Rodriguez-Serrano F (2014). Exosomes derived from breast cancer cells, small trojan horses? *J Mammary Gland Biol Neoplasia* **19**, 303–313.

[52] Hoshino A, Costa-Silva B, Shen TL, Rodrigues G, Hashimoto A, Tesic Mark M, Molina H, Kohsaka S, Di Giannatale A, and Ceder S, et al (2015). Tumour exosome integrins determine organotropic metastasis. *Nature* **527**, 329–335.